Title

Selective application of a TVD term to an implicit method

Journal

Journal of Flood Risk Management, 8(1)

ISSN

1753-318X

Authors

Ransom, O
Younis, BA

Publication Date

2015-03-01

DOI

10.1111/jfr3.12052

Peer reviewed

Journal of
Flood Risk Management

Selective application of a total variation diminishing term to an implicit method for two-dimensional flow modelling

O. Ransom and B.A. Younis

Department of Civil & Environmental Engineering, University of California, Davis, CA, USA

Correspondence
Owen Ransom, Department of Civil & Environmental Engineering, University of California, Davis, CA 95616, USA
Tel: +1 415 450 7558
Fax: +1 415 413 7558
Email: oransom@ucdavis.edu

DOI: 10.1111/jfr3.12052

Key words
Implicit; shallow water; shock capturing; total variation diminishing.

Abstract

An implicit method with selective total variation diminishing (TVD) term inclusion was developed and used to find solutions to the shallow water equations (SWEs) for free-surface flows in natural and engineered channels. The conservative form of the SWEs was employed, and the method incorporated an algorithm for selectively underrelaxing the iterative process to maintain stability and accuracy in the presence of shock interfaces. The value of the Courant number and the frequency at which the TVD term was incorporated were constantly updated during the computation to achieve optimal speed of execution while maintaining stability. The method was tested against published results from physical experiments and from computations employing alternative algorithms, and the results obtained demonstrate both the economy and accuracy of the proposed algorithm.

Introduction

The ability to capture shocks in the modelling of shallow water flows is important for scenarios involving the propagation of flood waves associated with levee failure and dam breaching. High-order explicit methods have been shown to be capable of capturing sharp discontinuities in shallow water solutions, especially when coupled with a total variation diminishing (TVD) term (Liang *et al.*, 2006). However, the time-step sizes are governed within an explicit scheme by the Courant–Friedrichs–Lewy (CFL) condition which imposes strict limits that are necessary to maintain the stability of the solution (Chaudhry, 2007). This limitation on the time-step size makes the use of explicit schemes computationally expensive and unsuited for real-time simulations or for carrying out the large number of computations needed to account for stochastic variability in the problem inputs (i.e. as part of a Monte Carlo simulations process). To avoid the restriction on time-step size, an implicit method that can capture shocks is preferable. Such a method would allow for faster solutions to large-scale problems, as the time step is not bound by CFL conditions, as fully implicit methods are unconditionally stable, and do not rely on the CFL to maintain stability. Typically, implicit methods have been prone to instability in the neighbourhood of sharp discontinuities (Rogers *et al.*, 2003; Liang *et al.*, 2006). This has led to the inclusion of artificial viscosity terms to stabilise the solutions (Davis, 1984), or more recently to the calculation of exact or approximate Riemann fluxes in conjunction with local characteristic decomposition in order to keep the methods stable and accurate at shock interfaces (Bermudez *et al.*, 1998; Rebollo *et al.*, 2003). Although the Riemann type solutions have shown good results, implementation is complex and computationally expensive (Delis *et al.*, 2000).

Recently, attention has been placed on developing methods that are numerically accurate, computationally efficient, and easy to implement (i.e. Delis and Katsaounis, 2005; Liang *et al.*, 2006; Liang *et al.*, 2007). These methods lend themselves well to large-scale engineering problems where a limited loss in accuracy and refinement around shocks is compensated for by significant speed-up in the computations. The relaxation scheme of Delis and Katsaounis (Delis, 2003; Delis and Katsaounis, 2005), and the explicit method of Liang *et al.* (2006; 2007) are modern schemes that compare well with Riemann-based solutions.

The current model demonstrates that selective inclusion of a TVD term into a finite difference implicit method can improve on the relaxation method of Delis and Katsaounis (2005) and the explicit limitations of Liang *et al.* (2006; 2007). The method solves the shallow water equations (SWEs) found by integration of the Navier–Stokes equations over the water column using the assumptions of hydrostatic

pressure distribution and the kinematic boundary condition of the free surface. A properly formulated finite-difference method allows solution of the weak conditions, creating a converging solution while also admitting discontinuities. The TVD term is introduced as needed to maintain stability and accuracy at the shock interface. The method is second-order accurate in both space and time; however, inclusion of the TVD terms reduces the method to first order around discontinuities.

Although the TVD term is important for maintaining stability, its application is not necessary at every time step, with overuse producing dissipative effects. The method includes the TVD term as necessary, based on the magnitude of the discontinuity within the solution domain. The method also adapts the Courant number *in situ*, increasing the time step as the solution domain smooths, and reliance on the TVD term for stability lessens.

Governing equations

For flows in natural domains, numerical instabilities have often been observed in shock-capturing methods, arising due to uneven bed topographies (Liang *et al.*, 2006). Moreover, inconsistent discretisation of the flux-gradient and source terms are common in cases where the water depth and discharge are the unknown. Following Rogers *et al.* (2003) and Liang *et al.* (2006), in order to more consistently discretise these terms, the deviatoric method is employed, where deviation from the still-water level and the discharge are taken as the variables of interest. Using this method proves more accurate not only during quiescent conditions, but during times of rapidly varied flow, or where complex bottom geometries are encountered. The general form, accounting for the deviatoric method, of the SWEs can be written as (Rogers *et al.*, 2003; Liang *et al.*, 2006):

$$\frac{\partial X}{\partial t}+\frac{\partial F}{\partial x}+\frac{\partial G}{\partial y}=E_x+E_y \tag{1}$$

where:

$$\mathrm{X}=\begin{bmatrix}\eta\\ q_x\\ q_y\end{bmatrix} \tag{2}$$

$$\mathrm{F}=\begin{bmatrix}q_x\\ \dfrac{q_x^2}{h+\eta}+\dfrac{g\eta^2}{2}+gh\eta\\ \dfrac{q_xq_y}{h+\eta}\end{bmatrix}\quad \mathrm{G}=\begin{bmatrix}q_y\\ \dfrac{q_xq_y}{h+\eta}\\ \dfrac{q_y^2}{h+\eta}+\dfrac{g\eta^2}{2}+gh\eta\end{bmatrix} \tag{3}$$

$$\mathrm{E_x}=\begin{bmatrix}0\\ g\eta\dfrac{\partial h}{\partial x}-\dfrac{gn^2q_x\left(q_x^2+q_y^2\right)^{1/2}}{(h+\eta)^2}\\ 0\end{bmatrix}$$

$$\mathrm{E_y}=\begin{bmatrix}0\\ 0\\ g\eta\dfrac{\partial h}{\partial y}-\dfrac{gn^2q_y\left(q_x^2+q_y^2\right)^{1/2}}{(h+\eta)^2}\end{bmatrix} \tag{4}$$

In the above, t is time, η is the deviation of the water surface elevation with respect to the still-water level, q_x and q_y are the discharge per unit width, h is the depth below the still-water datum, g is the gravitational acceleration, and n is Manning's n.

Numerical method

The implicit method utilised is based on a central differenced discretisation of the deviatoric formulation of the SWEs given in Eqns (1)–(4), and is second-order accurate in both time and space. Without special care, the method can generate spurious oscillations around areas that contain large gradients, as visible in Figure 2(c) and (d). Selective application of the presented TVD method was generally sufficient to eliminate or sufficiently dampen the oscillations inherent to the method as demonstrated in the Results and Discussion section. Underrelaxation (α) was used in conjunction with the TVD method to prevent over- and undershoots and further stabilise and speed completion of the iterative process. α is reported, if used, for simulations with very large velocity or depth gradients contained in this paper. The discretised two-dimensional equations, with included TVD and α terms, take the form:

$$\eta_{i,j}^n=\alpha\left(\eta_{i,j}^o-\frac{\Delta t}{2\Delta x}\left(q_{x_{i+1,j}}^n-q_{x_{i-1,j}}^n\right)-\frac{\Delta t}{2\Delta y}\left(q_{y_{i,j+1}}^n-q_{y_{i,j-1}}^n\right)\right)+(1-\alpha)\left(\eta_{i,j}^o\right)-TVD(\eta) \tag{5}$$

$$q_{x_{i,j}}^n=\alpha\left(q_{x_{i,j}}^o-\frac{\Delta t}{2\Delta x}\left(F_{i+1,j}^n-F_{i-1,j}^n\right)-\frac{\Delta t}{2\Delta y}\left(G_{i,j+1}^n-G_{i,j-1}^n\right)-\Delta t\left(E_{x_{i,j}}^n\right)\right)+(1-\alpha)\left(q_{x_{i,j}}^o\right)-TVD\left(q_x\right) \tag{6}$$

$$q_{y_{i,j}}^n=\alpha\left(q_{y_{i,j}}^o-\frac{\Delta t}{2\Delta x}\left(F_{i+1,j}^n-F_{i-1,j}^n\right)-\frac{\Delta t}{2\Delta y}\left(G_{i,j+1}^n-G_{i,j-1}^n\right)-\Delta t\left(E_{y_{i,j}}^n\right)\right)+(1-\alpha)\left(q_{y_{i,j}}^o\right)-TVD\left(q_y\right) \tag{7}$$

The superscripts *o* and *n* give the time level of the associated variable: *o* level values represent the previous time level, and *n* level values represent the most recent iteration. A series of equations dependent upon values from the current time level for calculation are created by applying Eqns (5)–(7) across all interior points of the domain. Therefore, the Gauss–Seidel iterative technique was chosen to solve for the unknown values η, q_x, and q_y. Because terms from Eqns (5)–(7) are interdependent, all three equations sets must be solved before a new iteration can begin. The Gauss–Seidel method iterates individually upon these systems of equations by calculating and successively replacing *n* level values for η, q_x, and q_y within the current time level until the individual total difference of all variables between the current and previous iteration fall below a preset number (E), set at 10^{-3} for the presented simulations. Only when this criteria is met do the *n* level values get written to the *o* level, and a time step is completed. A generic stencil showing the time step relationship between the *n* (current iteration) and *o* superscripted levels indicated in Eqns (5)–(7) is given in Figure 1:

Boundary conditions were obtained using the method of characteristics. In this method, the reflective boundary velocities and water depths were obtained from:

$$\Phi_e = v_{int}^n + \sqrt{\frac{g}{(h+\eta)_{int}^n}} \cdot q_{int}^n + E_{int}^n \cdot \Delta t \tag{8}$$

Where the subscripts *e* and *int* represent edge and immediate interior cells, respectively, and *E* can be found in Eqn (4). The new edge velocity then can be found following:

$$v_e^n = \Phi_e - \sqrt{\frac{g}{(h+\eta)_{int}^n}} \cdot (h+\eta)_{int}^n \tag{9}$$

The method proved adequate for boundary reflections, as evidenced in the two-dimensional results section.

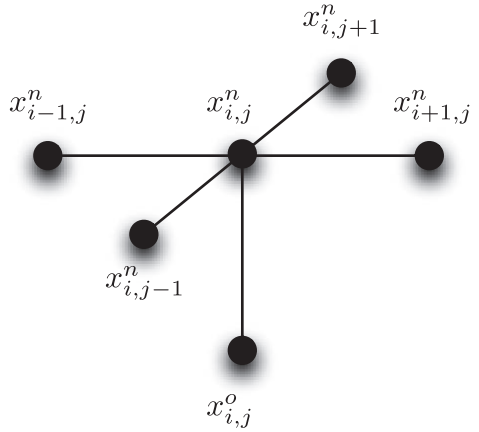

Figure 1 Stencil for the centre-differenced method employed in the current paper.

Adaptive TVD and Courant number calculation methods

The TVD method used was adapted from the research of Liang *et al.* (2006; 2007) for use within the framework of this scheme. The model was originally proposed by Davis (1984), and used for the solution of the SWEs by Louaked and Hanich (1998). The method was modified so that the predominant direction of flow dictates the terms used to determine the TVD correction. For a flow moving towards the coordinate origin, the TVD term takes on the form found in Eqn (10), otherwise the TVD term is as found in Eqn (11). Inclusion of this directional bias method improved the stability, measured as an increase in maximum stable Courant number, of the numerical method relative to a nondirectionally biased TVD term. The TVD method takes the form:

$$TVD_i = \left[G\left(r_i^+\right) + G\left(r_{i+1}^-\right)\right] \cdot \Delta X_{i+1/2}^n - \left[G\left(r_{i-1}^+\right) + G\left(r_i^-\right)\right] \cdot \Delta X_{i-1/2}^n \tag{10}$$

$$TVD_i = \left[G\left(r_{i+1}^+\right) + G\left(r_i^-\right)\right] \cdot \Delta X_{i+1/2}^n - \left[G\left(r_i^+\right) + G\left(r_{i-1}^-\right)\right] \cdot \Delta X_{i-1/2}^n \tag{11}$$

where X is initially defined in Eqn (2):

$$\Delta X_{i+1/2}^n = X_{i+1}^n - X_i^n \tag{12}$$

$$\Delta X_{i-1/2}^n = X_i^n - X_{i-1}^n \tag{13}$$

$$r_i^+ = \frac{\Delta\eta_{i-1/2}^n \cdot \Delta\eta_{i+1/2}^n + \Delta q_{x_{i-1/2}}^n \cdot \Delta q_{x_{i+1/2}}^n + \Delta q_{y_{i-1/2}}^n \cdot \Delta q_{y_{i+1/2}}^n}{\Delta\eta_{i+1/2}^n \cdot \Delta\eta_{i+1/2}^n + \Delta q_{x_{i+1/2}}^n \cdot \Delta q_{x_{i+1/2}}^n + \Delta q_{y_{i+1/2}}^n \cdot \Delta q_{y_{i+1/2}}^n} \tag{14}$$

$$r_i^- = \frac{\Delta\eta_{i-1/2}^n \cdot \Delta\eta_{i+1/2}^n + \Delta q_{x_{i-1/2}}^n \cdot \Delta q_{x_{i+1/2}}^n + \Delta q_{y_{i-1/2}}^n \cdot \Delta q_{y_{i+1/2}}^n}{\Delta\eta_{i-1/2}^n \cdot \Delta\eta_{i-1/2}^n + \Delta q_{x_{i-1/2}}^n \cdot \Delta q_{x_{i-1/2}}^n + \Delta q_{y_{i-1/2}}^n \cdot \Delta q_{y_{i-1/2}}^n} \tag{15}$$

Where G(x) is given as:

$$G(x) = 0.5 \times C \times [1 - \phi(x)] \tag{16}$$

and the flux limiter is given as:

$$\phi(x) = \max(0, \min(2x, 1)) \tag{17}$$

C is:

$$C = \begin{cases} C_l \times (1 - C_l), & C_l \le 0.5 \\ 0.25, & C_l > 0.5 \end{cases} \tag{18}$$

and finally *Cl*, the local Courant number:

$$C_l = \frac{\left(|q_x / H| + \sqrt{gH}\right)\Delta t}{\Delta x} \tag{19}$$

The use of the above TVD method requires no solution of eigenvalues or eigenvectors, reducing the number of computational steps needed per time step.

The TVD method is introduced in the solution at a rate that decreases as the solution smooths, and shocks diminish in the solution domain. Limiting TVD use maintains a sharp interface around shocks and bores while concurrently stabilising the numerical method. An empirical method has been developed for inclusion of the TVD term based on the presence of strong bores within the solution. The $G(x)$ term found in Eqn (16), which has the range [0, 0.25] is monitored from the first iteration and used to calculate the frequency of TVD inclusion (TVD_i). The term is calculated as the inverse average of all positive, nonzero values of $G(x)$ at a given time step multiplied by 0.25, as shown in the following pseudo-code example, and dictates the number of iterations that will occur until the TVD_i term is again incorporated into the method:

```
for i = (1,n_cells)
  if (Gx(i) > 0.0) then
    GXi_sum = GXi_sum+Gx(i)
    GXi_poscount = GXi_poscount+1
  end if
end for
```

$$\mathrm{TVD\_i} = \mathrm{integer}\left(\mathrm{floor}\left(0.25/\left(\mathrm{GXi\_sum}/\mathrm{GXi\_poscount}\right)\right)\right)$$

n_cells is the total number of cells in the domain, GXi_sum and GXi_poscount are reset to zero before each iteration, and TVD_i is rounded down to its integer value. The TVD operator is included on the first iteration, and then is included again in n iterations, where $n = TVD_i$.

The TVD terms and TVD_i are only calculated when dictated by TVD_i. For the tests included in this paper, this method has proved successful for maintaining stability and accuracy, even during times of strong shock propagation. Because the TVD method operates in transcritical areas by reducing the local solution from second to first order, applying the method a minimal number of times will minimise diffusion at the interface.

Figure 2 is a plot of a standard friction-free two-dimensional dam break scenario that has been used historically to analyse behaviour, accuracy, and shock capturing ability of SWE solution methods [(Louaked and Hanich, 1998; Liang *et al.*, 2006; Chaudhry, 2007) *et al.*]. Shown is the effect of differing levels of TVD application. As the application of the first-order TVD method decreases, the shock front steepens. Figure 2(a) shows the effect of applying the TVD method every iteration, resulting in a very smoothed solution, lacking characteristics generally found in transcritical flow. Figure 2(b) shows TVD_i using the method described above, which had an average application rate of once every nine iterations throughout the simulation run time. Figure 2(c) and (d) show further decreasing TVD use, and increasing instability can be observed. The goal of the variable TVD_i is to maintain a sharp transcritical flow region while damping nonphysical oscillations as seen in Figure 2(c) and (d).

Similar to the variable TVD term inclusion, the Courant number used for time step calculation is calculated in a manner to add to the efficiency of the present scheme. Although implicit methods are not bound to the CFL condition for stability purposes, proper Courant number choice will minimise the required number of iterations within a time step, therefore increasing the overall speed of the method. Two terms, C_{max} and C_{min} are dictated within the computer code, corresponding to the maximum and minimum allowable Courant numbers. The Courant number is then calculated by sweeping the domain with the following equation:

$$Courant = C_{\min} + \left[1 - 4 \cdot \max\left(\left|G(x)_{i+1} - G(x)_i\right|\right)\right] \cdot \left(C_{\max} - C_{\min}\right) \tag{20}$$

Where max() represents the maximum value obtained in the sweep of the domain. When C_{max} and C_{min} are chosen properly, this method monitors solution smoothness to apply a maximal time step, speeding computation time of the method, while maintaining accuracy and stability. Because all simulations in this paper contained strong shocks, a C_{min} of 0.4 and a C_{max} of 2.5 were used. Maximal (C_m) and average (C_{avg}) Courant numbers are reported for results within this paper.

Results and discussion

The current method was checked against experimental data and results from other simulations and analytical solutions for steady and unsteady flow problems. Most attention was given to problems that included a generated shock within the solution domain. The results are documented below.

Analytical comparison – one dimensional dam break

Following examples given in previous articles [(Tseng, 1999; Delis *et al.*, 2000; Lin *et al.*, 2003; Liang *et al.*, 2006) – (Benkhaldoun and Quivy, 2006) *et al.*], a one-dimensional dam break was analysed in order to measure the shock capturing ability of the current scheme. The test cases involved dam break scenarios that are usually used for the assessment of methods for shallow water computations. As the ratio between the water depth above and below the dam increases, the shock propagation speed also increases. Typically, implicit methods have difficulty maintaining stability at the transition zone, leading to oscillation, and eventually the divergence of the computations (Liang *et al.*, 2006). The current method was able to accurately predict the water surface elevation and shock propagation speeds, without oscillation, and at time step resolutions not bound by unity

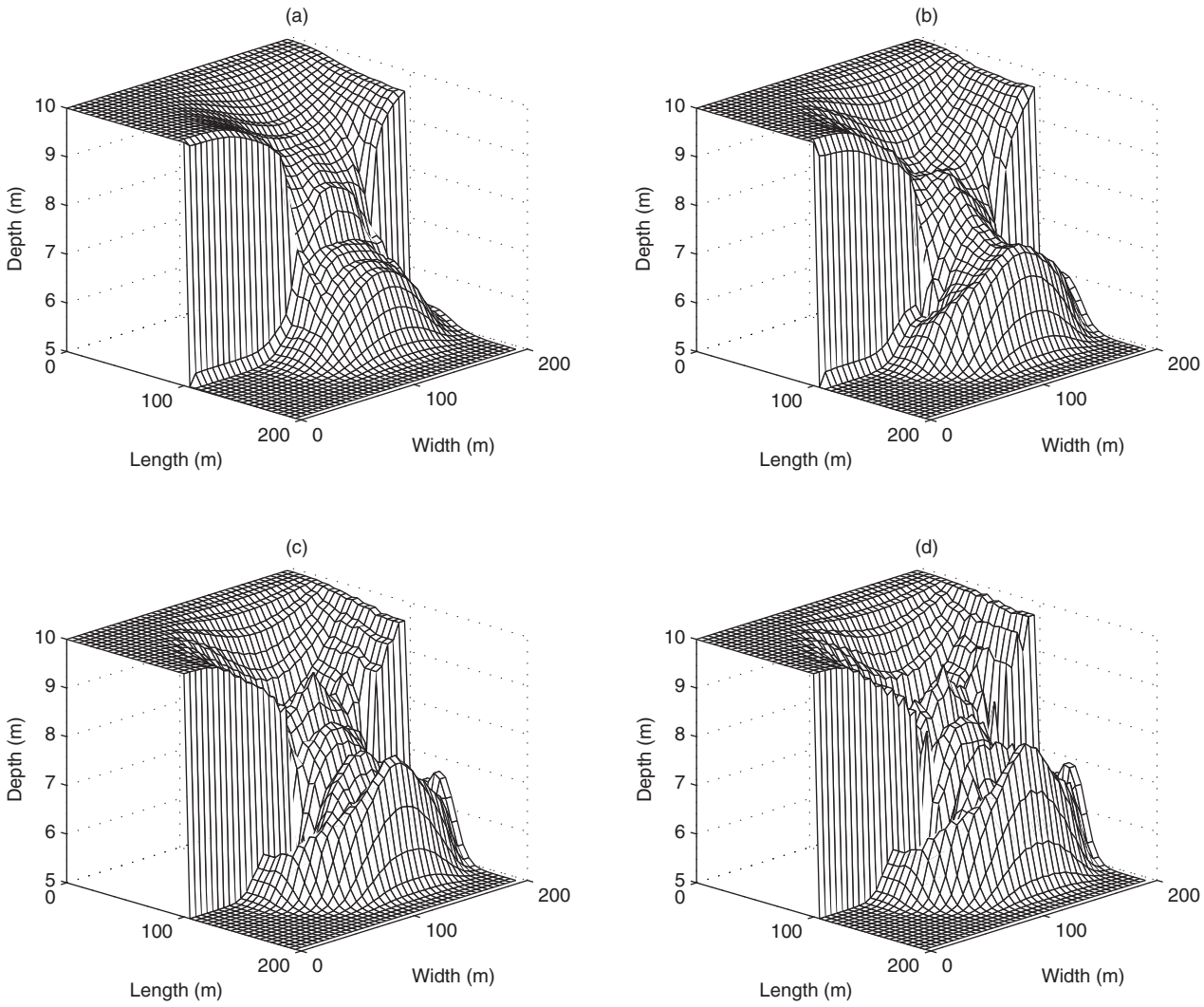

Figure 2 (a) TVD applied every iteration ($C_m = 2.5$, $C_{avg} = 1.95$) (b) TVD_i method application ($C_m = 2.5$, $C_{avg} = 1.84$) (c) every 30th iteration ($C_m = 2.26$, $C_{avg} = 1.27$) (d) every 50th iteration ($C_m = 1.71$, $C_{avg} = 0.93$).

of the CFL condition. Analytical solutions for total and instantaneous one-dimensional dam breaks have been obtained in Kim and Han (2000) and Liang *et al.* (2006), and are also included in the figures.

Figures 3–5 show comparison to the one-dimensional method initially found in Falconer (1986), where artificial viscosity was used to damp the oscillations. The channel has a length of 1000 m, and is slope and friction free. The dam bisects its length, with the upstream half having an initial water depth of 10 m, and the downstream half having a depth of 2 m, 0.1 m or 0.001 m. At time $t = 0$, the dam separating the two halves is instantaneously removed. Figures 3–5 show the method versus the analytical results of Liang *et al.* (2006) and the computations available in Chaudhry (2007) with both low and high artificial viscosity terms. Following examples in Delis *et al.* (2000) and Liang *et al.* (2006), Δx for each test case was 5 m. The current method exhibits none of the oscillatory or diffusive behaviour associated with use of artificial viscosity, while maintaining an accurate track on the advancing shock front. For Figures 3–6, the Courant number was in the range [0.4, 2].

Figure 6 shows the current method as tested against an Implicit – Essentially Non-Oscillatory scheme partially developed by Kim and Han (2000). The channel length is 2000 m, with an upstream depth of 10 m, and a downstream depth of 0.001 m. Again, the method compares favourably. A sharp front is maintained in the current method through use of the combination of the underrelaxation term and Courant number bracketing.

Finally, the one-dimensional dam break solution obtained using the current method was compared against a method utilising Roe's Riemann solver (Tseng, 1999; Lin *et al.*, 2003)

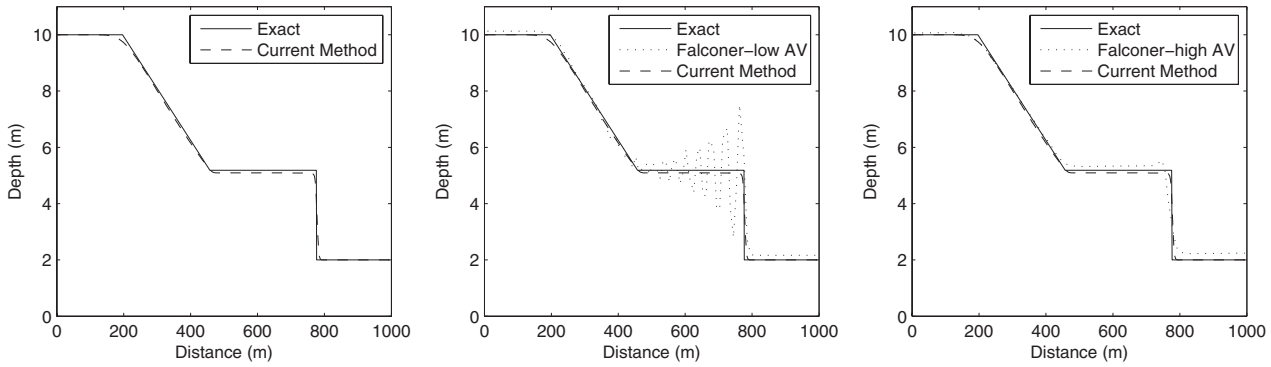

Figure 3 One-dimensional dam break: *ho* = *2 m* (C_m = 1.88, C_{avg} = 1.12).

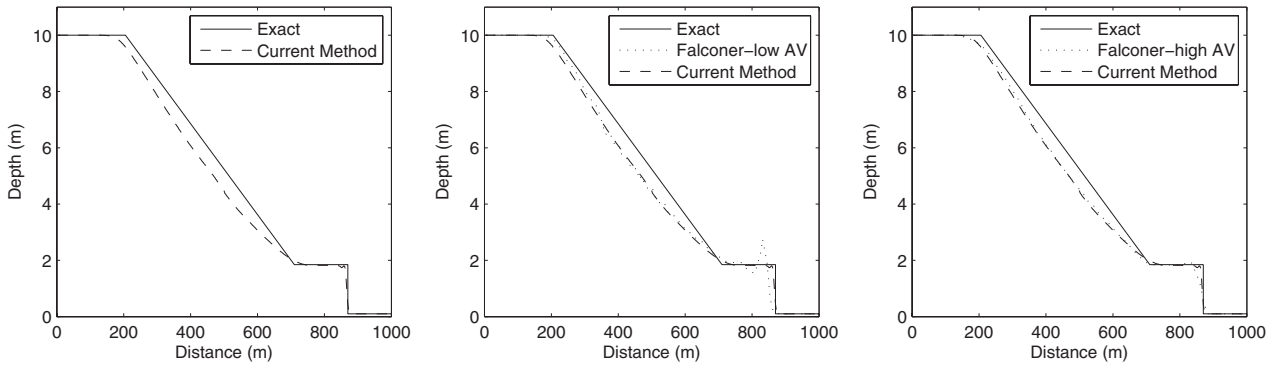

Figure 4 One-dimensional dam break: *ho* = 0.1 *m* (C_m = 1.52, C_{avg} = 0.86).

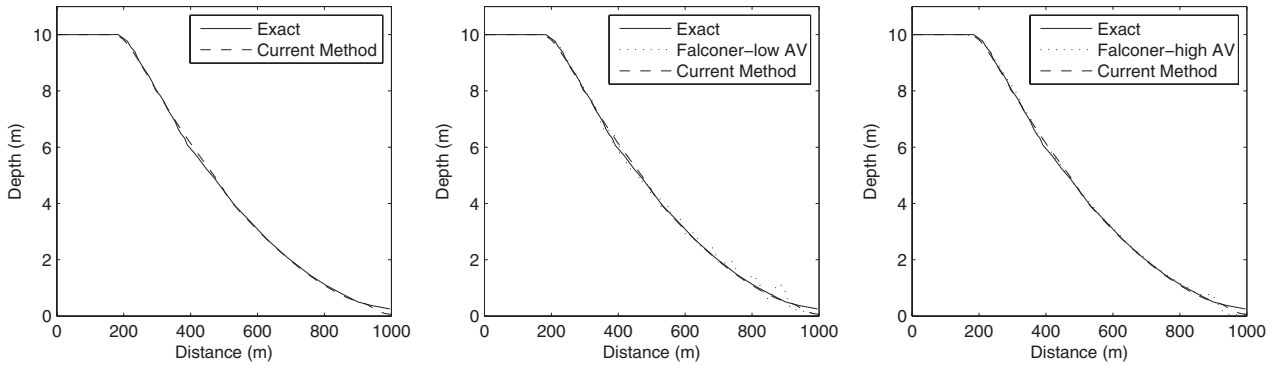

Figure 5 One-dimensional dam break: *ho* = 0.001 *m* (C_m = 1.48, C_{avg} = 0.82).

and a nonhomogeneous Riemann solver (Benkhaldoun and Quivy, 2006). For this example, an upstream depth of 6 m and a downstream depth of 2 m were used. Δx was set to 0.1 m. Results shown are for time $t = 0.4$ s. Although the Roe method is noniterative, it requires the computation of eigenvalues and eigenvectors making it more computationally inefficient than methods that do not rely on these computations (Tseng, 1999; Vincent *et al.*, 2000; Benkhaldoun and Quivy, 2006). The presented method compares favourably to both the Roe and nonhomogeneous Riemann methods, for a greatly reduced cost in complexity in comparison to the Riemann method while not requiring the computation of eigenvectors and eigenvalues necessary for the Roe method (Figure 7).

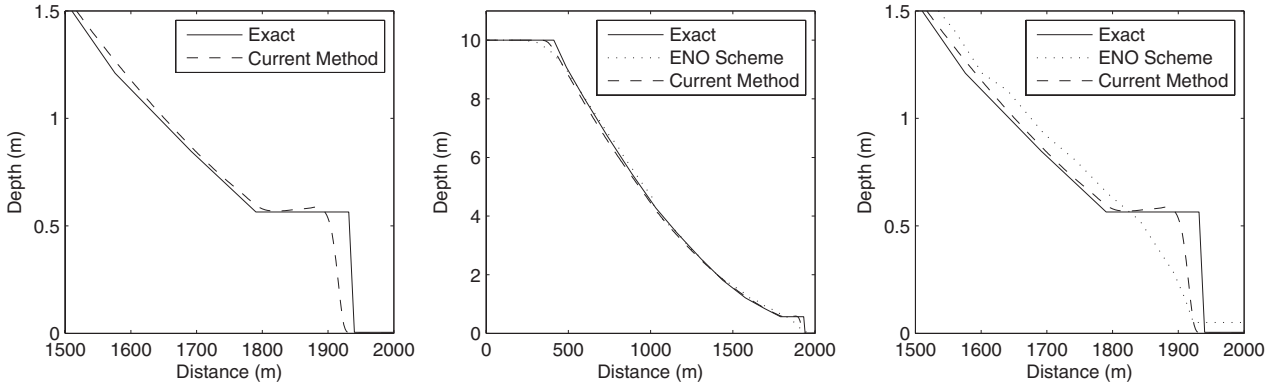

Figure 6 One-dimensional dam break: ENO method comparison, $\Delta x = 2$ m ($C_m = 1.48$, $C_{avg} = 0.82$).

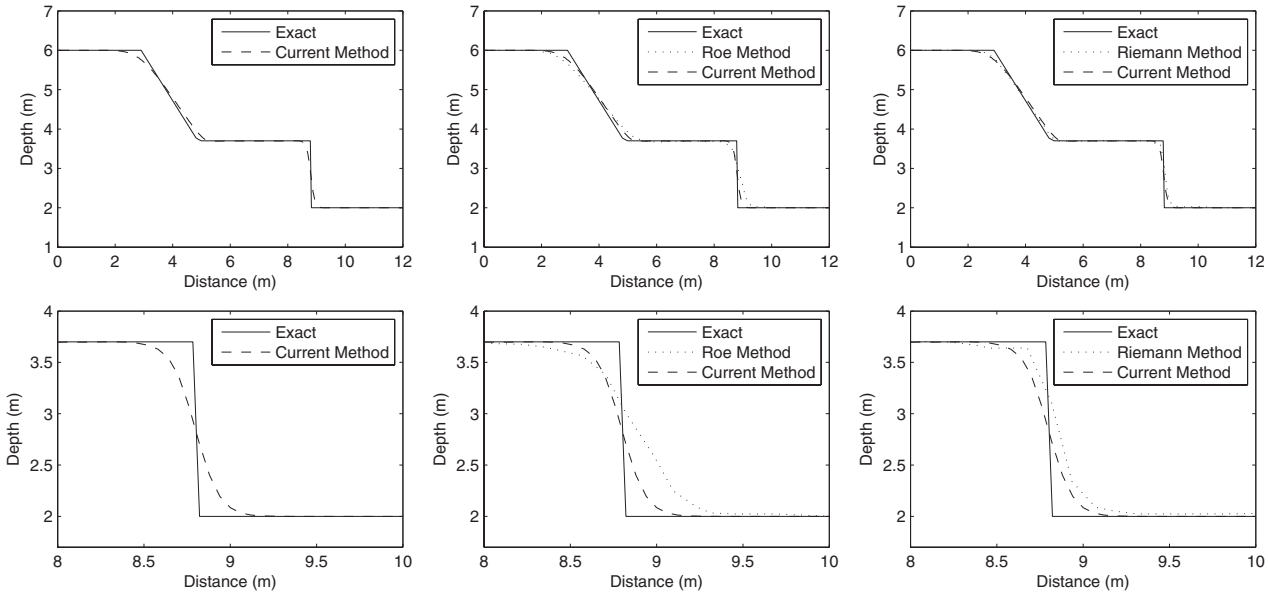

Figure 7 One-dimensional dam break: Roe and nonhomogeneous Riemann method comparison, ($C_m = 2.08$, $C_{avg} = 1.21$).

Physical comparison

The friction-free dam break models have analytical solutions that provide for excellent numerical solution comparison. However, comparisons to measured physical flow data obtained in real-world simulations can demonstrate a numerical method's ability to approximate flow when estimated parameters, such as Manning's n are used. To this end, the following one-dimensional and two-dimensional comparisons are based on laboratory-conducted experiments where flow was measured physically.

Dam break with bed friction

A 1960 test case carried out by the United States Army Corp of Engineers (USACE, 1960) is shown below. A physical model 122 m in length and 1.22 m in width was constructed that had a slope of 0.005 and a Manning's n of 0.009. A partition was inserted halfway, with an upstream water depth of 0.305 m. The dam was removed at $t = 0$ s. The propagating wave front is similar in nature to what is found in the friction-free test cases, but inclusion of friction will slow the shallow flow significantly, causing the front to quickly increase in depth as shown by the results computed using the current method.

Figure 8 shows the current method results against the measured results from the USACE test at $t = 5$ s, using a Δx of 1 m, an underrelaxation value $\alpha = 0.99$, and a bounded Courant number of [0.4, 2]. The accuracy of the current method is adequate, sufficiently tracking the increased water depth and wave propagation speed, and maintaining stability over a very thin flow with a significant friction factor.

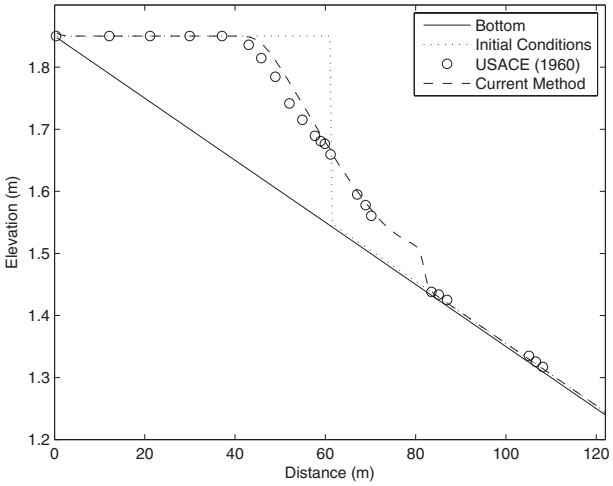

Figure 8 One-dimensional dam break: comparison against USACE (1960) results, ($C_m = 1.81$, $C_{avg} = 1.04$).

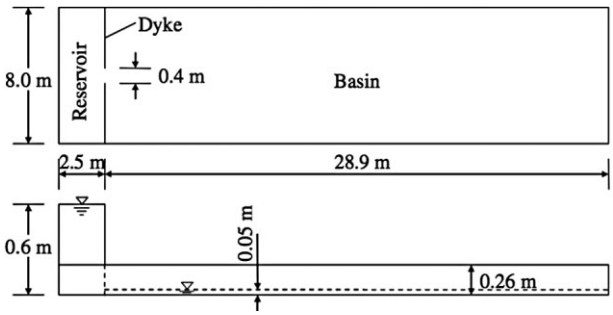

Figure 9 Geometry of the dyke-break experiment, taken from (Liang *et al*., 2007).

Errors in the upstream propagating wave may be the result of the lack of correction for the finite time it would take to remove the partition.

Two-dimensional dike break in a flume

The following dyke-break attempts to model the complex flow found in real-world flood wave propagation scenarios. A two-dimensional dyke break experiment was constructed in the Fluid Mechanics Laboratory at Delft University of Technology (Stelling and Duinmeijer, 2003). Figure 9 shows the geometry of the experiment. Manning's n was fixed at 0.012 across the domain, and Δx and Δy were both 0.1 m. For testing, the Courant number was in the range [0.4, 2.5].

The raising of the gate between the upstream and downstream water depths occurred at a relatively slow 0.16 *m/s*, necessitating special treatment within the code as follows (Stelling and Duinmeijer, 2003): The gate was opened in an upward direction. At the cells that bordered the gate, if the water level was higher than the gate opening, the gate boundary was treated as a solid wall. On the upstream end, the water level was fixed to 0.6, and velocities at the gate remained zero. On the downstream end, the boundary conditions were given as:

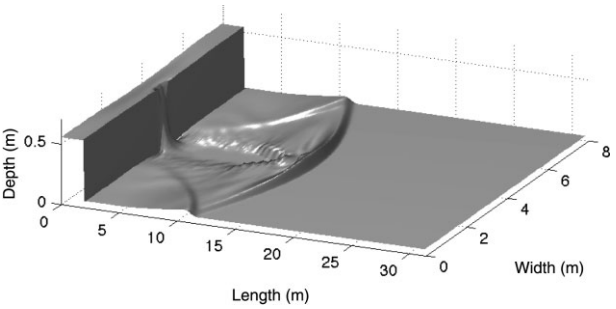

Figure 10 Dyke-break experiment, $t = 9$ s.

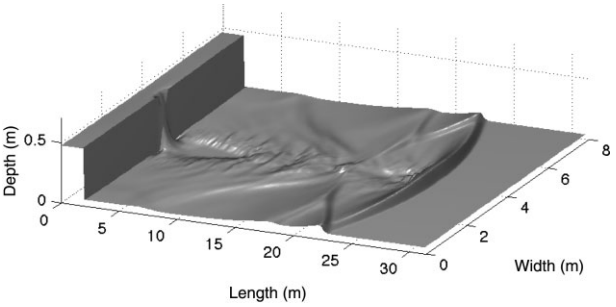

Figure 11 Dyke-break experiment, $t = 18$ s, ($C_m = 2.23$, $C_{avg} = 1.38$).

$$H = C_h \cdot h_G \tag{21}$$

$$q_x = C_h h_G \sqrt{2g\left(h_R - C_h h_g\right)} \tag{22}$$

$$q_y = 0 \tag{23}$$

where Ch is the contraction coefficient (0.6), hG is the height of the gate opening (t·0.16), and hR is the upstream water level (0.6 m) Immediately after the dike is initially broken ($t = 0$), a semicircular shock front propagates downstream, pushed by the jet of water from the breeched dike. A supercritical zone of flow is created behind the front, which eventually causes the creation of hydraulic jumps as the flow interacts with the walls and bottom of the solution domain. The supercritical zone and reflected bore is evident in Figure 10. As the solution is allowed to propagate, the initial circular bore spreads almost evenly across the width of the domain, as seen in Figure 11. The variety of flow regimes in this test shows the current schemes ability to predict sub-, trans-, and super-critical flow, all which exist in Figures 10 and 11. Measurements taken at gauging stations located at

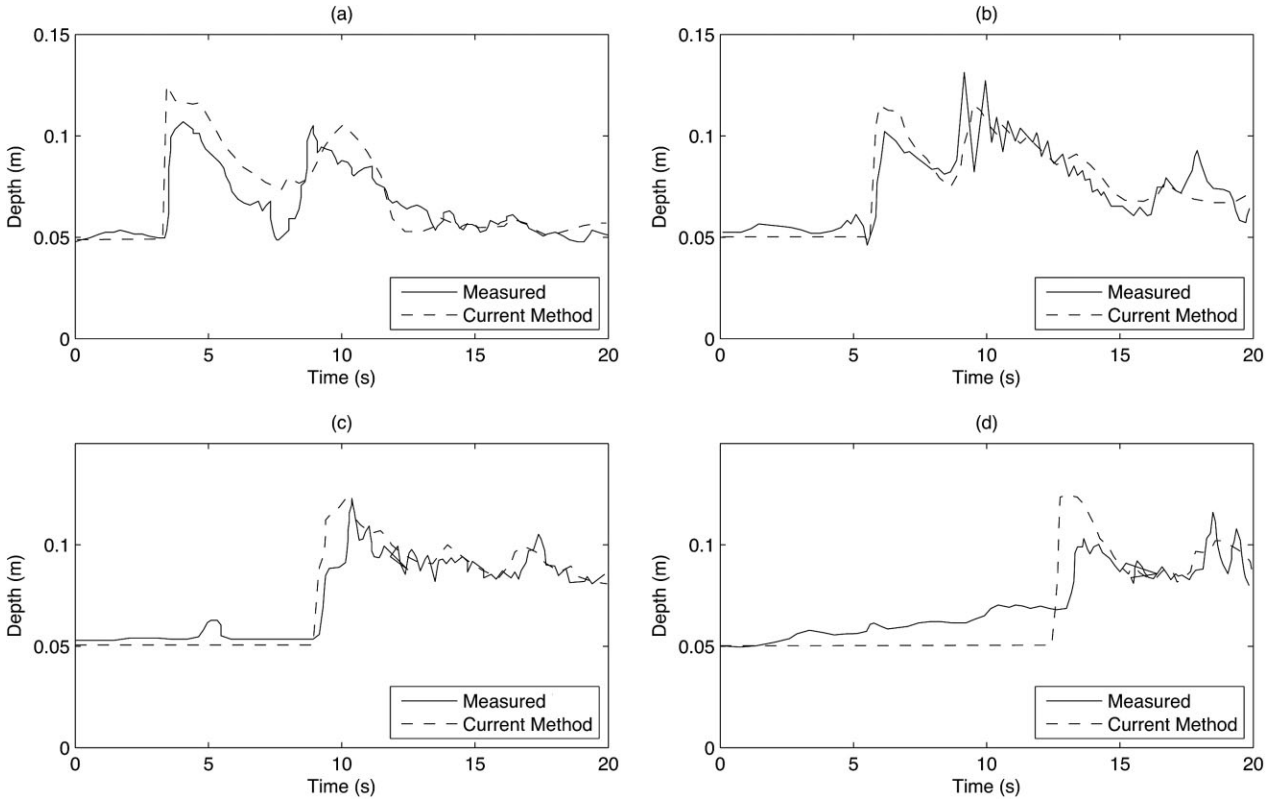

Figure 12 (a) gage station 6 m from the gate (b) 9 m from the gate (c) 13 m from the gate (d) 17 m from the gate.

6 m, 9 m, 13 m, and 17 m were compared against the computational results of the current method. Wave arrival times and evolution showed general agreement with the measured values, evident in Figure 12, and in comparison to previous results (Stelling and Duinmeijer, 2003; Liang *et al.*, 2004). The most significant deviation occurs from the measured data at the 17 m gauging station found in Figure 12(d), where the wave arrival time was 1 s early and off by 0.025 m. The method of characteristics boundary conditions utilised in the current method are unable to perfectly mimic the wave reflection detail or oscillation patterns found in the physical model, however wave reflection patterns compared well to the computational results in Liang *et al.* (2004). Generally, the lack of reflective wave detail should not greatly influence the accuracy of the current method with respect to prediction of flooding, except in cases where wave amplification may occur.

Conclusions

1. An implicit numerical scheme was formulated that utilised selective underrelaxation, a TVD term, and the deviatoric discretisation of the SWEs. The developed method was shown to exhibit good shock capturing characteristics.
2. The developed implicit method compared favourably with both explicit and implicit methods formulated expressly for transcritical flow prediction.
3. The scheme was able to at least match time step sizes of its explicit counterparts when shocks were present in the solution domain, and was able to maintain significantly larger time steps than the CFL condition would allow when the flow regime was gradually varied in the numerical field.
4. The method matched the accuracy of recently developed numerical methods that are more computationally expensive and more complex to code.
5. Adaptive time stepping and TVD term inclusion were used to minimise computational resources, and promote an overall faster code.
6. Using the adaptive TVD_i method damps oscillations around shocks and bores, but does not cause severe diffusive behaviour associated with constant TVD term application.
7. The current method has shown validity for both one- and two-dimensional flow, across all flow regimes, including those considered more extreme than would be expected in nature.
8. The model has promise as an efficient solution algorithm for transcritical flow regimes including shocks that were

previously the domain of explicit or computationally complex and expensive numerical schemes.

9. The method is robust and easy to implement, making it a valuable tool for numerical modelling of complex flow regimes.

References

Benkhaldoun F. & Quivy L. A non homogeneous Riemann solver for shallow water and two phase flows. *Flow Turbulence Combust* 2006, **76**, 391–402.

Bermudez A., Devieux A., Desideri J. & Vazquez M. Upwind schemes for the two-dimensional shallow water equations with variable depth using unstructured meshes. *Comput Methods Appl Mechan Eng* 1998, **155**, 49–72.

Chaudhry M. *Open-channel flow*, 2nd edn. New York: Springer Publishing Company, Incorporated, 2007.

Davis S. 1984). TVD finite difference schemes and artificial viscosity. Technical Report 84-20: ICASE.

Delis A. Improved application of the HLLE Riemann solver for the shallow water equations with source terms. *Commun Numer Methods Eng* 2003, **39**, 59–83.

Delis A. & Katsaounis T. Numerical solution of the two-dimensional shallow water equations by the application of relaxation methods. *Appl Mathemat Model* 2005, **29**, 754–783.

Delis A., Skeels C. & Ryrie S. Implicit high-resolution methods for modeling one-dimensional open channel flow. *J Hydr Res* 2000, **38**, (5), 369–382.

Falconer R. Water quality simulation study of a natural harbor. *J Water Port Coast Ocean Eng ASCE* 1986, **112**, (1), 15–34.

Kim W. & Han K. Computation of transcritical flow by implicit eno scheme. In ICHE, editor, 4th International Conference on Hydro-Science and Engineering, 2000.

Liang D., Falconer R. & Lin B. Comparison between TVD-MacCormack and ADI-type solvers of the shallow water equations. *Adv Wat Resour* 2006, **29**, 1833–1845.

Liang D., Lin B. & Falconer R.A. Simulation of rapidly varying flow using an efficient TVD-MacCormack scheme. *Int J Numer Methods Fluids* 2007, **53**, 811–826.

Liang Q., Borthwick A. & Stelling G. Simulation of dam- and dyke- break hydrodynamics on dynamically adaptive quadtree grids. *Int J Numer Methods Fluids* 2004, **46**, 127–162.

Lin G.-F., Lai J.-S. & Guo W.-D. Finite-volume component-wise TVD schemes for 2D shallow water equations. *Adv Wat Resour* 2003, **26**, 861–873.

Louaked M. & Hanich L. TVD scheme for the shallow water equations. *J Hydr Res* 1998, **36**, (3), 363–378.

Rebollo T., Delgado A. & Nieto E. A family of stable numerical solvers for the shallow water equations with source terms. *Comput Methods Appl Mechan Eng* 2003, **192**, 203–225.

Rogers B., Borthwick A. & Taylor P.H. Mathematical balancing of flux gradient and source terms prior to using roe's approximate Riemann solver. *J Comput Phys* 2003, **192**, 422–451.

Stelling G. & Duinmeijer S. A staggered conservative scheme for every Froude number in rapidly varied shallow water flows. *Int J Numer Methods Fluids* 2003, **43**, 1329–1354.

Tseng M. Explicit finite volume non-oscillatory schemes for 2D transient free-surface flows. *Int J Numer Methods Fluids* 1999, **30**, 831–843.

USACE. Floods resulting from suddenly breached dams. Technical report, U.S. Army Engineer Waterways Experiment Station, Corps of Engineers, Vicksburg, Mississippi, 1960.

Vincent S., Caltagirone J.P. & Bonneton P. Numerical modeling of bore propagation and run-up on sloping beaches using a MacCormack TVD scheme. *J Hydr Res* 2000, **39**, (1), 41–49.

